Pergamon

Journal of Structural Geology, Vol. 18, Nos 2/3, pp. 265 to 279, 1996

0191-8141/96 $15.00 + 0.00

0191-8141(95)00118-2

Changes in fault displacement populations correlated to linkage between faults

STEVEN F. WOJTAL

Department of Geology, Oberlin College, Oberlin, OH 44074, U.S.A.

(*Received* 13 *January* 1995; *accepted in revised form* 31 *August* 1995)

Abstract—In Carboniferous strata exposed at the western margin of the southern Appalachian (U.S.A.) fold–thrust belt, mesoscopic faults accommodated strains as the Cumberland Plateau thrust sheet moved ≤ 1 km WNW on a sub-horizontal detachment. These faults are confined to a layer ~75 m thick above the detachment. In the upper part of this ~75 m thick layer, a laterally persistent coal seam separates two stratigraphic units subjected to different amounts of sub-horizontal elongation. Distinct sets of mesoscopic faults that cut bedding at high angles and have normal offsets accommodate the strains in each unit.

Below the coal seam, a sample line ~500 m long intersects 504 faults. A plot of log N (size rank) vs log d (dip separation in mm) for these faults is linear, suggesting that a scaling law $N = ad^{-c}$ holds for this population. Least-squares regression gives $c \approx 0.8$ and $\log_{10} a \approx 3.1$. Above the coal seam, a sample line ~250 m long intersects 745 faults. A plot of log N vs log d for these faults has two distinct linear trends. Faults with separations ≤ 1.25 m yield a scaling law $N = ad^{-c}$ with $c \approx 0.5$ and $\log_{10} a \approx 2.9$. Seventeen faults with separations $d \geq 1.25$ m define a second linear segment $N = a' d^{-c'}$, with $c' \approx 1.8$ and $\log_{10} a' \approx 6.9$. The break in slope at $d \approx 1.25$ m corresponds to faults with heights of ~30 m, roughly equal to the thickness of the faulted strata. Faults here with $d \leq 1.25$ m and $d \geq 1.25$ m, which exhibit different scaling characteristics, are, respectively, analogous to faults within and those that extend across the brittle crust in regional studies.

Comparing the two displacement populations described here, small-offset faults make a proportionally smaller contribution to the total strain in the larger strain setting. This pattern, which is observed elsewhere, suggests that fault systems within individual layers exhibit different scaling characteristics at different stages in their history. This contribution argues that fault linkage is the key to such changes in fault scaling behavior; it is a mesoscopic to macroscopic structural change that alters the subsequent development of faults. Fault linkage, like fault size or sampling dimension, should be considered in examinations of fault scaling laws.

INTRODUCTION

Individual faults in isotropic media grow in a self-similar or self-affine manner, with characteristic scaling laws relating fault length, fault width (or height), fault thickness and the magnitude of fault slip (Watterson 1986, Walsh & Watterson 1988, Marrett & Allmendinger 1990, 1992, Scholz & Cowie 1990). Geometric similarity leads to power-law scaling for size-frequency distributions in fault populations (Villemin & Sunwoo 1987, Scholz & Cowie 1990, Marrett & Allmendinger 1991, 1992, Cowie & Scholz 1992a,b, Jackson & Sanderson 1992). For faults that follow power-law scaling.

$$N = AD^{-C_1}, \quad (1)$$

where N is the numerical rank of each fault in a list ordered by slip magnitude, D is the slip magnitude on that fault, and A and C_1 are constants (see Marrett & Allmendinger 1991, Westaway 1994). In this case, a plot of log N vs log D, a *displacement population* in the terminology of Marrett & Allmendinger (1992), will define a straight line with a slope of $-C_1$ and with an intercept on the ordinate equal to log A.

Departures from self-similar or self-affine fault growth can occur. The scaling relationship between the thickness of fault zones and fault slip magnitude may change, for example, when deformation mechanisms in fault rocks or fault slip mechanisms change in response to microstructural changes wrought during early slip increments (Wojtal & Mitra 1986, 1988, Hull 1988). A more subtle possible effect is a change in fault scaling parameters that occurs as fault populations evolve. Small faults make proportionally smaller contributions to the total strain as the strain magnitude increases (Kakimi 1980, Wojtal 1986, 1994), which leads to, or is reflected in, shallower slopes on log N vs log D plots. This effect is subtle because variations in sampling dimension may give the appearance of changing scaling characteristics (Marrett & Allmendinger 1991, Marrett 1996) and the size range of the faults may correlate with a systematic change scaling behavior (Nicol *et al.* 1996). Finally, displacement populations for limited size ranges may develop breaks in slope as fault link and/or interact; the positions of breaks in slope identify critical length scales such as the dimensions of layers that control the deformation (Wojtal 1994). Departures from linearity on log N vs log D plots, if due to linkage, suggest that linked fault systems differ geometrically from individual fault strands, i.e. have different ratios of overall length to width (or height), have different distributions of total slip (Peacock & Sanderson 1991), or different degrees of surface complexity (Okubo & Aki 1987). Cartwright *et al.* (1995) and Dawers & Anders (1995) have discussed how fault linkage can influence the displacement–length scaling relationship for faults. In this contribution, I investigate the effect of fault interaction and linkage on fault size–frequency distributions.

In order to examine correlations between strain mag-

nitude, fault linkage and fault scaling behavior, I collected size–frequency data for two distinct fault populations in two sedimentary units exposed at a single location in the southern Appalachians (U.S.A.). A thin coal seam separating the two units is a locus of structural disharmony. Neither faults nor folds persist across the coal seam, and the units above and below it experienced different amounts of sub-horizontal elongation. I collected fault data along two sample lines, one below the coal seam and one above it. Despite the common structural setting, the uniform sampling technique, and the similar rock types and fault geometries above and below the coal seam, the two populations have markedly different size–frequency distributions. In this contribution, I consider whether the observed differences between the two samples arise from subtle differences in fault geometry or from the inadvertent sampling of two or more distinct fault populations in one sedimentary nit, or are artifacts due to differences in sampling rates for faults of different sizes (cf. Marrett 1996). My analysis indicates that the differences in fault scaling behavior are real, and I argue that these changes result from the interaction and linkage of faults. Finally, in light of these results, I examine the utility of size–frequency scaling relationships as a means of characterizing and distinguishing fault populations.

FAULT POPULATIONS

Geologic setting

The fault populations described here occur in Pennsylvanian conglomerates, sandstones and shales exposed in the Cumberland Plateau in Tennessee, U.S.A. (Fig. 1a). The Cumberland Plateau in Tennessee is underlain by a blind thrust fault that cuts up-section to the west from the regional décollement in Cambrian strata to a detachment horizon in Pennsylvanian strata. A ramp anticline formed above the fault step (Milici 1963), and erosion removed resistant Pennsylvanian strata from the crest of the anticline to create the Sequatchie Valley (Fig. 1b). Erosion in the Sequatchie Valley is sufficiently deep that the thrust itself was also breached. An ESE-dipping thrust ramp, with Ordovician limestones thrust on Mississippian strata, now crops out along the west side of the valley floor; a sub-horizontal detachment, with Pennsylvanian strata thrust on other Pennsylvanian strata, intersects the escarpment along the west side of the valley (Figs. 1a & b). Displacement at the thrust ramp is 2–3 km but decreases up the dip of the fault so that slip on the blind upper detachment is 300–1000 m (Harris & Milici 1977). The transport direction inferred for the Cumberland Plateau thrust sheet is 280° (Wojtal 1986, Wojtal & Pershing 1991). During its WNW-directed movement, arrays of mesoscopic faults formed in strata within ~75 m of the upper detachment (Harris & Milici 1977, Wojtal 1986).

A series of road cuts along Tennessee route 8, which follows a stream valley incised in the west side of Sequatchie Valley, provides more than 2 km of continuous exposure across the pervasively-faulted layer at the base of the Cumberland Plateau thrust sheet (plate 3 in Harris & Milici 1977). Beginning where the road grade crosses the sub-horizontal, blind upper detachment, the road takes ~1 km to climb, along a curved path, through the lowermost 75 m of the thrust sheet; the western ~1 km of exposures run nearly across strike and roughly parallel to the sub-horizontal detachment and its sub-horizontal enveloping strata, providing a view of transport-parallel changes in thrust-related deformation (Fig. 2). Within this ~75 m thick deformed layer are one set of mesoscopic faults that cut bedding at low angles (≤45°) and at least two sets of mesoscopic faults that cut bedding at high angles (≥45°). Exposures yield clear views of separations of bedding across faults; slickensides are preserved on some fault surfaces. Where 'drag' folds or small extension veins exist in strata adjacent to faults, they conform with the measured offsets and with the slip sense inferred from slickensides on faults. One cannot, however, rule out multiple movement directions on faults. This uncertainty is vexing, but similar difficulty in inferring displacement affects all studies of inactive faults.

Low-angle faults throughout the ~75 m thick deformed layer have down-dip lineations and reverse offsets of bedding (Wojtal 1986). About 500 m west of where the road crosses the detachment, and 50–60 m above the detachment, several low-angle reversal faults have asymptotic intersections with a superjacent thin coal seam (between A and B on Fig. 2). The seam persists more than 1 km to the west, but pinches out to the east. Low-angle faults are very rare in the sandstones and conglomerates just above the coal seam (between B and C on Fig. 2), but there is a contractional duplex with top-to-the-WNW slip in shales at the top of the deformed layer exposed at the west end of the road cuts (at D on Fig. 2).

Within 50 m of the detachment, high-angle faults cut both bedding and low-angle reverse faults. Those high-angle faults nearest the detachment (within 10 m of it) have cross-strike to obliquely-inclined lineations and both normal and reverse offsets of bedding and low-angle faults (Wojtal 1986). Farther from the detachment (between 10 and 50 m above it), high-angle faults have obliquely-inclined to down-dip lineations and consistently normal offsets of bedding and low-angle faults, i.e. they are extension faults (Norris 1958). Whereas low-angle faults predominate in sandstones and siltstones beneath the coal seam between A and B on Fig. 2, extension faults predominate in these strata between B and C on Fig. 2. High-angle extension faults between B and C on Fig. 2 typically have NE strikes and SE or NW dips (Fig. 3a). Lineations on these faults pitch between 0° and 90°, so slip normals (Price 1967, Wojtal 1986) for these faults have shallow to steep, mainly NE, plunges (Fig. 3b).

Neither the low-angle faults between A and B on Fig. 2 nor the high-angle extension faults between B and C on Fig. 2 cut or offset the coal seam. Likewise, folds in

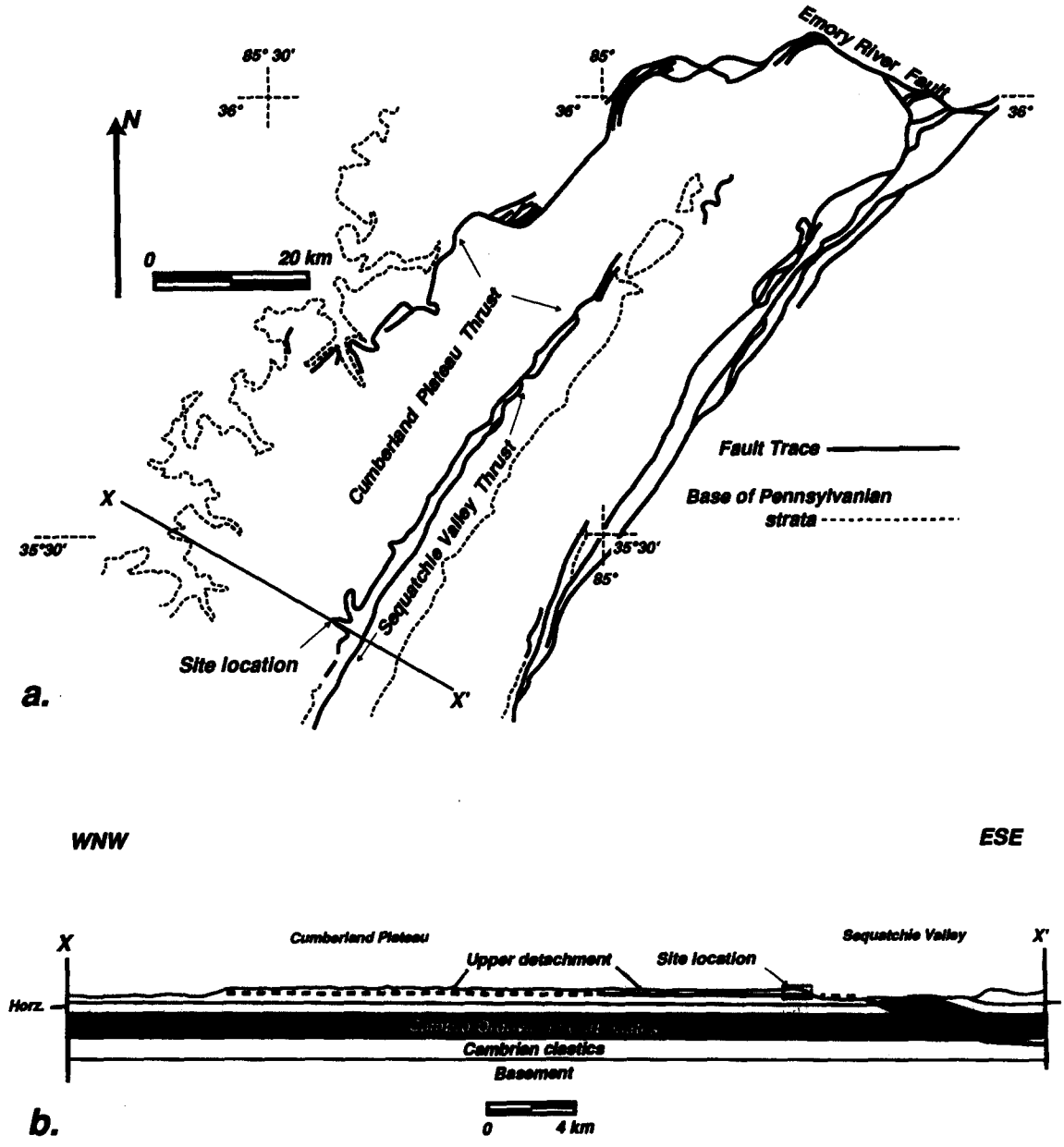

Fig. 1. (a) Map of the major faults of the Cumberland Plateau region of east Tennessee, U.S.A., after Rodgers (1953) and Milici (1963). X–X′ gives the line of section for (b). (b) Cross-section (with no vertical exaggeration) of the Cumberland Plateau region, showing the Cumberland Plateau thrust stepping from a regional décollement in Cambrian strata to an upper detachment in Pennsylvanian strata. Dashed box at west side of the Sequatchie Valley gives the location of exposures described here.

strata beneath the seam do not affect the seam or strata above it. The seam itself is pinched and swollen, and joints in the coal, especially those visible in the swells, have sigmoidal shapes consistent with top-to-the-WNW slip. This coal seam is, therefore, a bedding-parallel fault and is the locus of a significant strain discontinuity. Sandstones and conglomerates immediately above the coal seam (between C and D on Fig. 2) are also cut by high-angle faults with normal offsets of bedding, i.e. extension faults. Extension faults in strata above the coal seam (between C and D on Fig. 2) have, however, NNE strikes and mainly W dips (Fig. 3c). These faults have mainly down-dip lineations, so slip normals for the faults cluster about a horizontal, NNE-trending line (Fig. 3d). While high-angle extension faults above and below the coal seam have similar traces across rock faces and in a transport-parallel profile (Fig. 2), they are geometrically and kinematically distinct.

Extension faults below the persistent coal seam

With the excellent exposure and the finely stratified nature of the sandstones and siltstones below the coal seam, numerous faults are apparent. One can usually discern offsets of bedding smaller than a millimeter. For this analysis, I measured the dip separation of bedding across each of the 504 faults that intersected a sub-horizontal test line in a 510 m traverse along the exposure face (the test line extended roughly from B to C on Fig. 2). The maximum dip separation of bedding on an extension fault below the coal seam is 1.3 m; most faults have dip separations on the order of centimeters

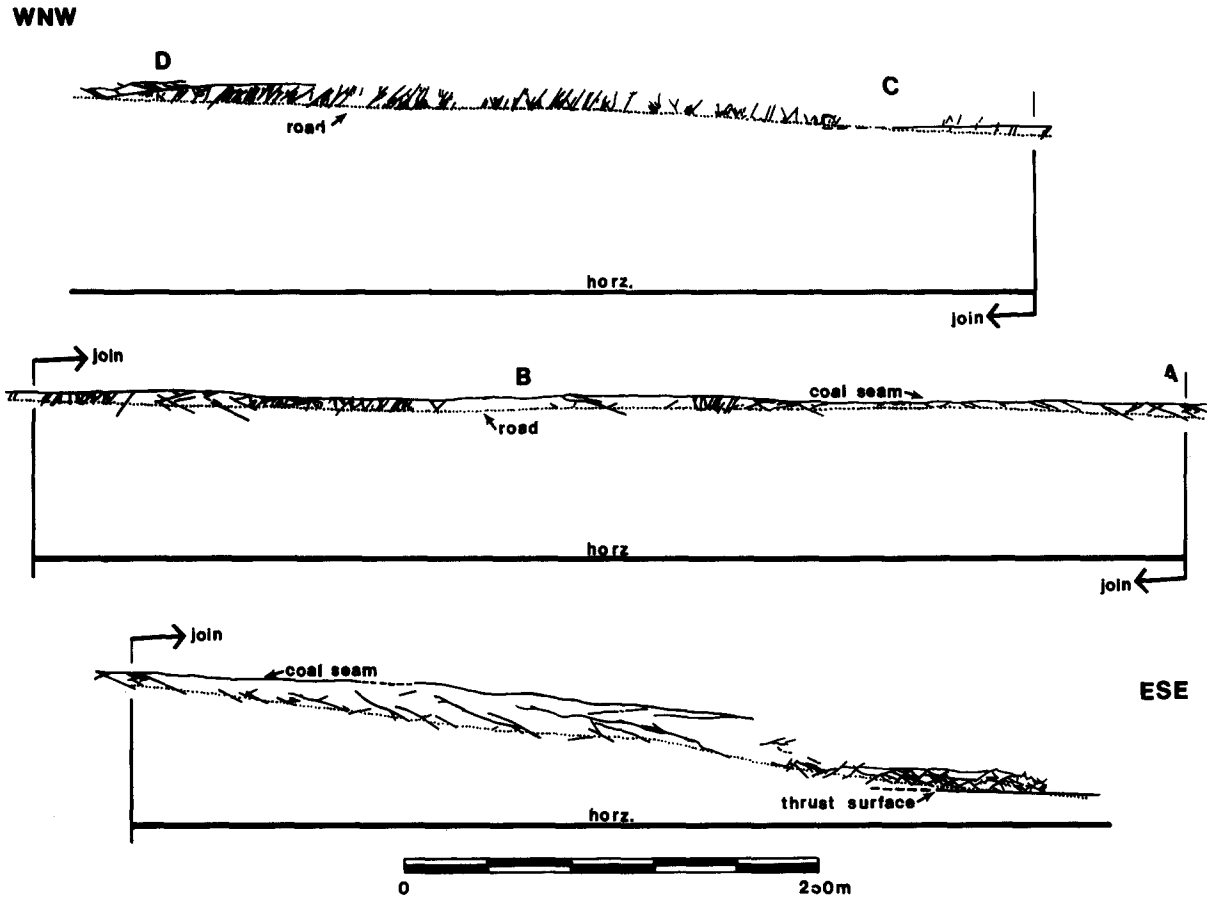

Fig. 2. Profile of the pervasively-faulted strata exposed along Tennessee route 8, showing faults that persist for at least 1 m across outcrop face. The profile plane is vertical and has a strike of 110°; horizontal and vertical scales are equal. Individual structural features were located on a plane table map, and then were plotted after projecting their positions along a horizontal line normal to the thrust transport and normal to profile plane. The profile geometry of faults at the ESE end of the profile may differ somewhat from their field appearance because exposures there are not generally parallel the profile plane. From A to the west, exposures are roughly parallel to the profile plane and the profile geometry is quite similar to that seen in field exposure faces. Between A and C, steeply-dipping faults resembling those shown between C and D are visible in the steep exposure faces above the coal seam. These faults were inaccessible, could not be located precisely and therefore are not shown.

or millimeters. In order to minimize the effects of 'binning' in compiling and plotting these separation data, I recorded small separations to the nearest millimeter.

Figure 4 is a log N vs log d plot, where N is the numerical rank of a fault in a list ordered by magnitude of measured offset and d is the measured dip separation for that fault, constructed from these data (all log–log plots presented here use logarithms to the base 10). I included all faults with separations $\leq$ 5 mm in one category and arbitarily plotted N for this category at d = 2.5 mm. The data points on Fig. 4 define a line, implying that

$$\log N = -c \log d + \log a \qquad (2)$$

or that $N = a\,d^{-c}$. Since data points corresponding to the smallest separation classes and the largest separation faults plot below this linear trend, the numbers of faults with the smallest and the largest separations might be under-sampled somewhat (cf. Marrett & Allmendinger 1990). The values of c and log a change only slightly, however, on excluding different small separation classes and large separation faults from least-squares regressions of the log N vs log d plot, suggesting that under-sampling is slight. Using all data for a least-squares regression, c = 0.857 and $\log_{10} a$ = 3.095 with the correlation coefficient r = 0.980. Excluding the six smallest separation classes (faults with $d \leq 1$ cm, see Fig. 4) and the two largest separation faults yields c = 0.812 and $\log_{10} a$ = 3.067 with r = 0.993.

As a way of further characterizing this fault population, I measured fault density below the coal seam. The average number of faults pierced by a unit length of test line (P_L) is a function of the overall density of faults in these strata; P_L = 0.998 m^{-1}. If fault surfaces were perfectly oriented and the test line were normal to the faults rather than parallel to bedding and inclined 65–75° to the faults, fault surface area per unit volume $S_V = 2P_L$ (Underwood 1970, pp. 66–71). Assuming, for argument, than the faults were perfectly oriented and all were inclined 70° to layering,

$$S_V = \frac{2P_L[\text{parallel to bedding}]}{\cos[90° - 70°]} \approx 2\,\text{m}^{-1}. \qquad (3)$$

In detail, of course, fault surface area per unit volume varies from position to position along these exposures.

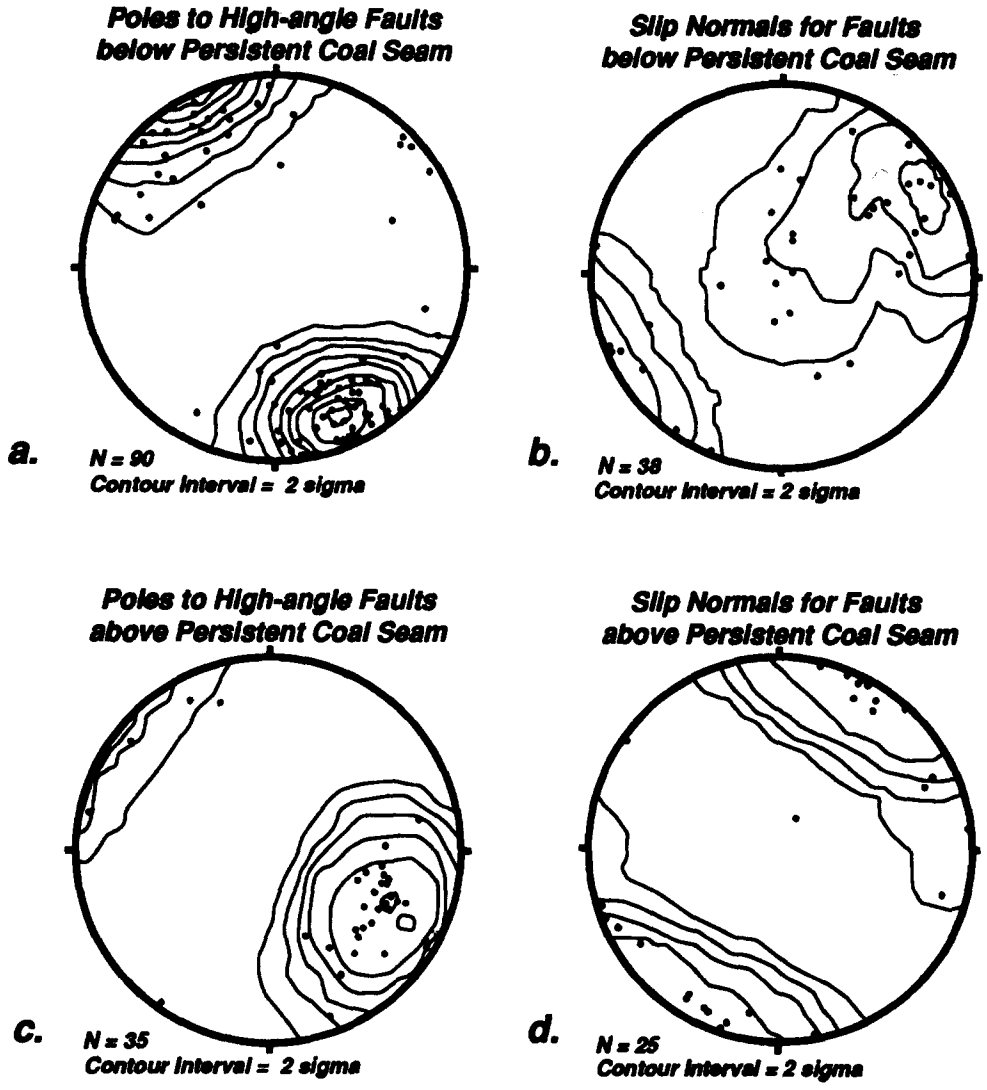

Fig. 3. (a) Contoured lower-hemisphere, equal-area projection of poles to high-angle faults below the persistent coal seam. (b) Contoured lower-hemisphere, equal-area projection of slip normals (Price 1967, Wojtal 1986) for high-angle faults below the persistent coal seam. (c) Contoured lower-hemisphere, equal-area projection of poles to high-angle faults above the persistent coal seam. (d) Contoured lower-hemisphere, equal-area projection of slip normals for high-angle faults above the persistent coal seam. Contours were drawn following the method given by Kamb (1959).

An assessment of the clustering of faults in this population is beyond the scope of this analysis, but the great length of the test line (several hundred meters) relative to the typical spacing of faults (at most tens of meters) minimizes the effects of clustering of faults on this 'bulk' value of fault surface area per unit volume. Fault surface area per unit volume calculated in this way is necessarily, however, a crude measure of fault density. Moreover, fault surfaces are not perfectly oriented. Measurement of the surface area per unit volume of partially oriented surfaces requires at least two perpendicular test lines; for features in a partially oriented, planar orientation, it is $S_V = P_L(\perp) + P_L(\parallel)$ (Underwood 1970, pp. 66–71), where $P_L(\perp)$ denotes the number of planes pierced by a test line normal to the orientation plane and $P_L(\parallel)$ denotes the number of planes pierced by a test line parallel to the orientation plane. Taking the orientation plane to be normal to bedding and parallel to mean fault strike, $S_V \approx 6.7$–$18\ m^{-1}$ in the vicinity of large-offset faults. Elsewhere, areas of at least 4 m^2 have $S_V \approx 0\ m^{-1}$.

The low value of the 'bulk' fault surface area per unit volume and the generally low magnitudes of separations on faults suggest that the magnitude of strain accommodated by these faults is low. Using the method outlined in Wojtal (1989), I constructed displacement diagrams, determined the magnitudes of displacement gradients and calculated a bulk strain for these faulted strata. These oblique- to normal-slip high-angle faults accommodated less than 1% elongation parallel to bedding and parallel to the WNW-trending transport direction, less than 1% shortening normal to bedding, and mean shear strains parallel to bedding of ~0.02.

Extension faults above the persistent coal seam

In the thickly-bedded sandstones or conglomerates above the persistent coal seam (between C and D on Fig.

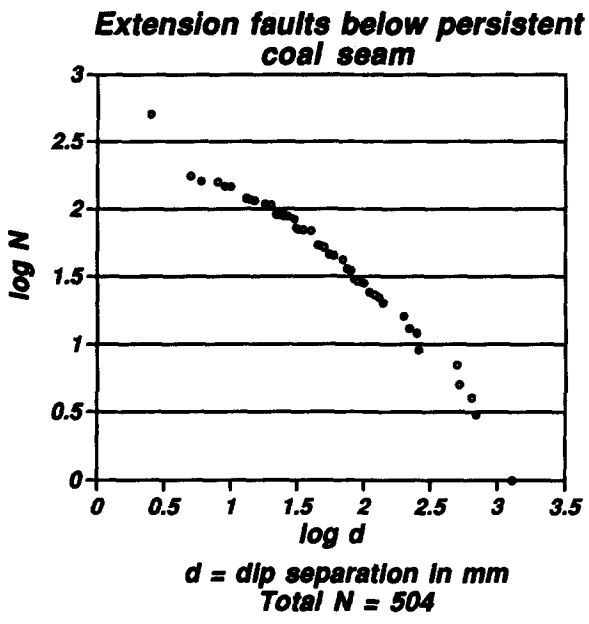

Fig. 4. Plot of log N, where N is the numerical rank of a fault in a list ordered by magnitude of measured offset, vs log d, where d is the dip separation of that fault measured in mm, for 504 faults in strata beneath persistent coal seam. All faults with $d \leq 5$ mm constitute the smallest separation class; the next five separation classes are 5, 6, 8 mm (i.e. no faults intersected by traverse have $d \approx 7$ mm), 9 mm and 1 cm. Data define a line; least-squares regression gives −0.8 as the approximate slope of the line.

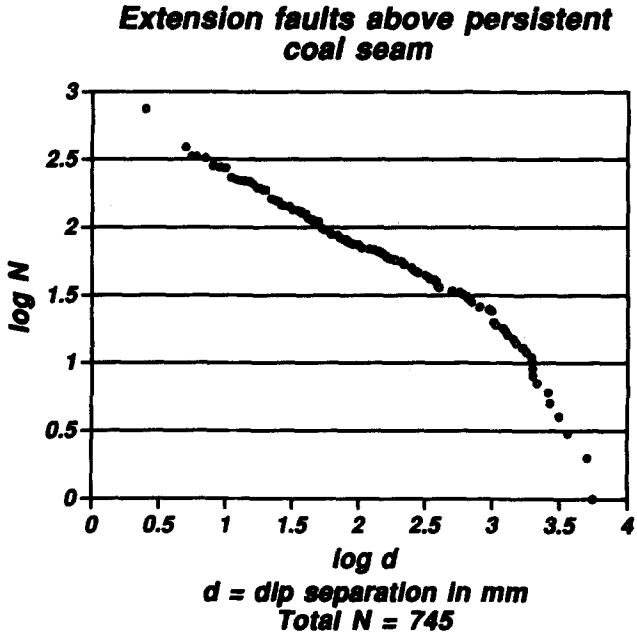

Fig. 5. Plot of log N vs log d for 745 faults in strata beneath persistent coal seam. All faults with $d \leq 5$ mm constitute the smallest separation class; the next five separation classes are 5, 5.5, 6, 7 and 8 mm. For some of the faults with separations ≥ 2 m, I was unable to identify in the field the hangingwall and footwall cut offs of a single bed; in these cases, the d value was found by examining a small-scale cross-section of the deformed strata. I used the maximum d value compatible with the small-scale section in order not to underestimate slip on large faults. Data fall along two lines; least-squares regression gives −0.5 and −1.8 as the approximate slopes of the lines.

2), it was sometimes difficult to identify hangingwall and footwall cut-offs of a single bedding plane in order to measure separations on small-offset faults. At most locations, however, faults cut and offset thin shale or siltstone beds in the sequence, making it possible to identify clearly both cut-offs. I measured or estimated dip separations across each of the 745 faults that intersected a sub-horizontal test line in a 247 m traverse along the exposure face (the test line extended two-thirds of the distance from D to C on Fig. 2). The maximum dip separation on a high-angle normal fault above the coal seam is 5.6 m, and separations on several high-angle normal faults exceed 1 m. Still, most faults have dip separations on the order of centimeters or millimeters. In order to minimize the effects of 'binning' in compiling and plotting these separation data, I again recorded small separations to the nearest millimeter.

Figure 5 is a log N vs log d plot constructed from these data; I again included all faults with separations ≤ 5 mm in one category and arbitrarily plotted N for this category at $d = 2.5$ mm. Faults with separations ≤ 1.25 m define a line, indicating that $\log N = -c \log d + \log a$ or that $N = ad^{-c}$. Even the data for the smallest separation classes conform to this linear trend, so the values of c and $\log a$ change only very slightly on excluding small separation classes in a least-squares regression of the log N vs log d plot. However, 17 faults with $d > 1.25$ m fall significantly below this linear segment. Using data for all faults with $d \leq 1.25$ m (and therefore excluding the 17 largest separation faults) in a least-squares regression, $c = 0.529$ and $\log_{10} a = 2.939$ with the correlation coefficient $r = 0.997$. Excluding the smallest separation class and the 17 largest separation fault yields $c = 0.525$ and $\log_{10} a = 2.925$ with $r = 0.998$. The 17 faults with the largest separations define a different linear segment, with $\log N = -c' \log d + \log a'$ or $N = a'd^{-c'}$. A least-squares regression of these data gives $c' = 1.815$ and $\log_{10} a' = 6.937$ with $r = 0.985$.

Considering fault density above the persistent coal seam, the average number of faults pierced by the test line in these strata is $P_L = 3.009\ \text{m}^{-1}$. Assuming, for argument, that these fault surfaces too were perfectly oriented and the test line was normal to the faults rather than parallel to bedding and inclined 60–70° to the faults, fault surface area per unit volume,

$$S_V \approx \frac{2P_L[\text{parallel to bedding}]}{\cos[90° - 65°]} \approx 6.5\,\text{m}^{-1}. \quad (4)$$

Using the equations for partially oriented, planar orientation features from Underwood (1970) and again taking the orientation plane to be parallel to mean fault strike and normal to bedding, $S_V \approx 62\ \text{m}^{-1}$ in areas of high fault density in these strata. Areas where $S_V \approx 0\ \text{m}^{-1}$ rarely exceed 1 m^2.

The average fault surface area per unit volume in strata above the coal seam is more than three times that below the seam, and large separations faults are more numerous. Together these observations suggest that the magnitude of strain accommodated by faults above the coal seam is sizable. I constructed displacement diagrams for these faulted strata, determined the magnitudes of displacement gradients, and calculated the bulk strain (Wojtal 1989) in these strata. These normal-slip

high-angle faults accommodated ~12% elongation parallel to bedding and parallel to the WNW-trending transport direction, ~20% shortening normal to bedding, and a mean shear strain parallel to bedding of ~0.17.

DISCUSSION

Inferring scaling laws from log N *vs log* d *plots*

There are two interrelated reasons for compiling displacement populations. The first is a desire to understand the geometric character of faults. The $N = AD^{-c_1}$ scaling law for displacement populations is explicitly related to scaling laws between fault length and width or between fault length and displacement (Marrett & Allmendinger 1991, Cowie & Scholz 1992a,b). Comparing displacement populations in different geologic settings may help illuminate whether and how fault geometries change as fault populations evolve. The second is the desire to use data collected over a limited range of lengths to constrain inferences on fault frequencies or strain magnitudes at other length scales (Scholz & Cowie 1990, Walsh *et al.* 1991, Westaway 1994, Wojtal 1994). Clearly, it is desirable to know how reliable are the scaling parameters inferred from data like log N vs log d plots. Two factors must be considered in assessing specifically the reliability of scaling parameters derived from Figs. 4 and 5: the relationship between the separation (d) measured on a fault and its displacement (D) and the effects of sampling technique on faults of different sizes.

Fault separation data and displacement populations. The size–frequency scaling law proposed for fault populations relates the number of faults (ΣN) to the displacement on them (D). On the extension faults considered in this contribution, I was able to measure separations (d) not displacements. This situation is comparable to many other studies, where 'displacement populations' are compiled using heaves or throws of faults measured on seismic sections (e.g. Childs *et al.* 1990, Walsh *et al.* 1990, Marrett & Allmendinger 1992, Westaway 1994). Measured separation values must scale uniformly to slip magnitudes on the faults in order for c, the slope of the log N vs log d plots (i.e. Figs. 4 and 5), to correspond to a one-dimensional measurement of the parameter relating the numbers of small faults in an area to the number of large faults (C_1'' of Marrett & Allmendinger 1991 or c_1 of Westaway 1994). Measured separations of bedding depend on the relative orientations of the slip direction and the trace of bedding on the fault surface (Redmond 1972). In the faulted strata considered here bedding is everywhere sub-horizontal, giving similar bedding traces on all faults. The separation of bedding depends, then, on slip direction. True displacement on a fault (D) is related to the dip separation (d) on the fault by

$$D = d/\sin p = d \operatorname{cosec} p, \quad (5)$$

where p is the pitch of the slip direction, normally

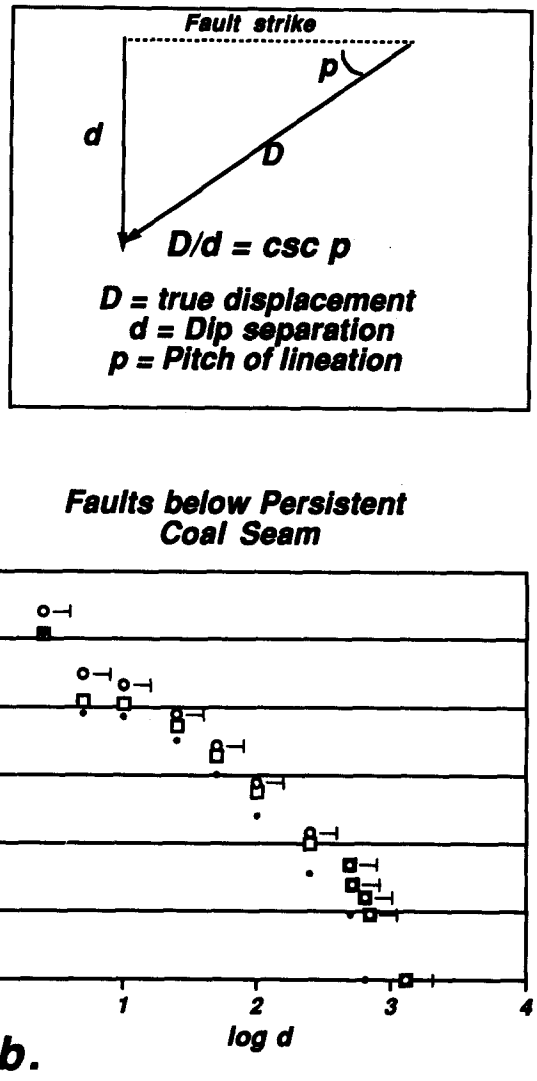

Fig. 6. (a) View of a fault surface showing that the relative magnitudes of true displacement, D, and dip separation, d, depend upon the pitch p of the slip direction. (b) log N vs log d plot for faults below the persistent coal seam. The large open circles denote the raw counts of faults. The 'error bars' extend from log d to log (1.56d), the maximum range of D for moderate and large offset faults. The open squares denote a 'residual' extension fault population derived by subtracting a strike-slip fault population with $C_1'' = 1.0$. The small, filled circles denote a 'residual' extension fault population derived by subtracting a strike-slip fault population with $C_1'' = 0.7$. See text for explanation.

inferred from the pitch of slickenside lineations on a fault (Fig. 6a). Substituting equation (5) into equation (1) written in logarithmic form and with parameters for one-dimensional sampling (Marrett & Allmendinger 1991) yields

$$\log N = -C_1'' \log (d \operatorname{cosec} p) + \log A$$
$$= -C_1'' \log d - C_1'' \log (\operatorname{cosec} p) + \log A. \quad (6)$$

Comparing equations (2) and (6) shows that $c = C_1''$ only if

$$\log a = -C_1'' \log (\operatorname{cosec} p) + \log A. \quad (7)$$

If slip directions on faults have uniform pitches, then p is the same for all faults, and a, the inverse logarithm of the intercept of the log N vs log d plot, will be constant as long as A is constant. In practice, slip directions on faults within a population will have a range of pitches. As long

as the variation in p is neither systematic nor dependent upon D, a 'displacement population' derived from separation data will yield a reasonable estimate of the intrinsic scaling parameter C_1''.

Some faults included in the samples presented here have quartz-fiber lineations. If the direction of slip on a fault did not change during its slip history, lineations indicate the fault's slip direction (Ramsay & Huber 1983, p. 258, Twiss & Moores 1992, pp. 61–62). In deformed strata from the Cumberland Plateau thrust zone, minor 'drag' folds and subsidiary faults or fractures typically have orientations consistent with the inference that lineations parallel the net slip direction. Unfortunately, not all faults sampled here possess lineations or subsidiary 'drag' structures.

Of the high-angle faults above the coal seam that possess lineations, nearly all have lineation pitches >70° (Table 1); all faults with $d > 50$ cm have lineations that pitch more than 70° or drag structures indicating dip-slip movement. I infer then that dip separation is a reliable estimate of true slip on high-angle faults above the coal seam, that the log N vs log d plot in Fig. 5 accurately represents a displacement population for those faults, and that c (or c') is a reliable estimate of C_1'' of Marrett & Allmendinger (1991) or c_1 of Westaway (1994). Mineral lineations on high-angle faults in strata below the persistent coal seam, however, have a range of pitches (Table 1). There are three possible reasons for the observed variation in the pitch of lineations on faults below the coal seam.

(i) All high-angle faults were active at the same time, and each fault had a single, uniform slip direction. The range of lineation pitches indicates that slip direction varied from fault to fault, consistent with kinematically-linked dip-slip and strike-slip faults or consistent with an elongation of bedding during non-plane strain.

(ii) Slip occurred on all high-angle faults at the same time, but slip direction varied with position on some or all faults due to large fault length-width ratios, interactions between neighboring faults, or, to a lesser degree, variations in rock properties (Pollard *et al.* 1993). In this case, bed-parallel fault zones like the upper detachment of the Cumberland Plateau thrust, the persistent coal seam, and the duplexed shale are likely to affect significantly slip directions on mesoscopic faults.

(iii) High-angle faults with different slip directions were active at different times in the deformation of these rocks.

Wojtal & Pershing (1991) examined faults throughout the 75 m thick deformed zone and found that high-angle normal faults and low-angle reverse faults in these strata conformed with different 'paleostress' or incremental strain tensors. High-angle and low-angle fault populations probably were active at different times. Considering only high-angle faults below the coal seam, slip normals to these faults define a single diffuse great circle, suggesting that they were active concurrently (Arthaud 1969). One best-fit tensor Wojtal & Pershing (1991) reported is compatible with high-angle faults possessing a range of lineation orientations, but that incremental strain tensor is not compatible with all high-angle faults in these strata. Slip on some individual extension faults could have re-oriented neighboring faults, thereby rendering them incompatible with a bulk incremental strain tensor. The relatively small magnitudes of fault displacements below the coal seam indicate that block rotation is unlikely to have caused all the variation in the pitch of slickensides. A cluster analysis of faults here distinguished an additional (third) incremental strain tensor compatible with high-angle faults in these strata (Nemcok & Lisle 1995), but this tensor is poorly-defined. Different parts of individual extension faults could have experienced different slip directions, i.e. hypothesis (ii) could hold. In the case here, simultaneous top-to-the-WNW slip on the coal seam and elongation of beds beneath it would cause changes in slip directions on portions of extension faults near the coal seam. A sub-horizontal traverse a few meters below the coal seam would, in that case, cross geometrically-similar and simultaneously-active faults of different sizes at different relative distances from the coal seam, resulting in a range of observed lineation pitches. Slip directions on interacting faults differ from the maximum resolved shear stress by as much as 40°, but angular discrepancies are usually ~10° in areas of low fault density (Pollard *et al.* 1993). Angular discrepancies on interacting faults vary smoothly from low to high values, however. The total number of measured lineations is too small to support definite conclusions, but the paucity of measured lineations with moderate pitches (Table 1) suggests that the variation of lineation pitches is not due to fault interactions. In summary, the population in Fig. 4 may be composed of two distinct populations of high-angle faults, but, at a minimum, dip separation does not scale uniformly with displacement on these faults.

I endeavored to assess the error in wrongly assuming that dip separation scales uniformly with displacement for faults below the coal seam. The 26 faults with lineation pitches $p > 40°$ (Table 1) have $d \geq 10$ cm. For these 'large-offset' faults, $d \leq D \leq d \operatorname{cosec} 40° = 1.56d$. Taking $D \approx d$ for small offset faults, $D \approx 1.56d$ for the moderate offset faults, and ignoring faults with $d \geq 50$ cm, the shallowest straight line that conforms with the log N vs log d plot has a slope $c \approx 0.75$ (Fig. 6b).

Assessing the possibility that the sample contains a mixture of extension fault and strike-slip fault populations is more difficult. Table 1 indicates ~32% of all slickensided faults below the coal seam are strike-slip faults. If those data are representative of the population as a whole, as many as 160 of the 504 faults below the coal seam could be strike-slip faults. Because faults with $d > 10$ cm have lineations with $p > 40°$, strike slip faults must be disproportionately represented in small offset classes. In the absence of lineation measurements for all 504 faults, however, it is not clear which 160 small-offset faults are strike-slip faults. If the hypothetical strike-slip displacement population followed power-law scaling, $\log N = -C_1'' \log D + \log A = -C_1'' \log d - C_1'' \log (\operatorname{cosec} p) + \log A$ for that population. Marrett & Allmendinger

Table 1. Distribution of pitches (p) of measured lineations on high-angle faults below and above the persistent coal seam. For high-angle faults below the coal seam, ~68% of the measured lineations indicate dip-slip movement and ~32% of the measured lineations indicate strike-slip movement. For high-angle faults above the coal seam, 92% of the measured lineations indicate dip-slip movement and 8% of the measured lineations indicate strike-slip movement. The ratio of the true displacement to the measured dip separation, D/d = cosec p (Fig. 6), gives the size of the factor by which one must multiply the dip separation in order to find the true displacement

	Faults below coal seam		Faults above coal seam		
Range of lineation pitches	Number	%	Number	%	D/d = cosec p
$p \leq 10°$	6	~16	0	—	> 5.75
$10° < p \leq 20°$	5	~13	1	4	$5.75 \geq D/d \geq 2.9$
$20° < p \leq 30°$	1	~3	1	4	$2.92 \geq D/d \geq 2$
$30° < p \leq 40°$	0	—	0	—	$5 \geq D/d \geq 1.55$
$40° < p \leq 50°$	4	~10	0	—	$1.55 \geq D/d \geq 1.31$
$50° < p \leq 60°$	3	~8	0	—	$1.31 \geq D/d \geq 1.15$
$60° < p \leq 70°$	4	~10	0	—	$1.15 \geq D/d \geq 1.06$
$70° < p \leq 80°$	2	~5	6	24	$1.06 \geq D/d \geq 1.01$
$80° < p \leq 90°$	13	~34	17	68	$1.01 \geq D/d \geq 1$
Total	38		25		

(1991) note that $0.37 \leq C_1' \leq 1$. Taking the size rank $N = 160$ for $d < 5$ mm, C_1'' must be greater than 0.7 or else the maximum separation expected on faults is greater than 3 m, more than twice the observed maximum separation on any fault and more than 30 times the maximum observed separation on any fault with a lineation with a low pitch. Taking $0.7 \leq C_1'' \leq 1$ for the hypothetical strike-slip fault population and $N = 160$ for $d = 1$ mm, one can calculate the numbers of faults in different separation classes and subtract that number from the raw counts in different separation classes. Assuming that the 'residual' fault counts are representative of an extension fault displacement population below the coal seam, the smallest magnitude of the scaling parameter for extension faults is $C_1' = 0.65$, found by taking $D \approx d$ for small offset faults, $D \approx 1.56d$ for all moderate offset faults, and ignoring faults with $d \geq 50$ cm (Fig. 6b). Considering faults in all separation ranges, the scaling parameter for the residual extension faults $C_1'' \approx 0.8$ (Fig. 6b).

It is worthwhile to assess critically the magnitude of the slope of the log N vs log d plot determined for this population ($c = 0.812$–0.857; $C_1'' \approx 0.65$–0.8), especially considering that typically $C_1'' \approx 0.5$ (Marrett & Allmendinger 1991). Three possible tests come to mind. First, using the values of c and $\log_{10} a$ determined from a best-fit line through the data, one can estimate the maximum dip separation that might be expected for a fault in this fault population by setting $-c \log_{10} d_{Max} + \log_{10} a = 0$. The best-fit values of c and $\log_{10} a$ from Fig. 4 suggest that $d_{Max} \approx 4$–6 m in this population. Given the structural setting of these deformed strata, above a thrust with a net slip of 100–300 m and in pervasively-faulted rocks where the maximum observed slip on any fault is less than 15 m (Wojtal 1986), the predicted maximum separation is reasonable. Second, one can: (1) assume $d_{Max} = 10$ m is the upper limit in these strata; (2) assume $c \approx 0.5$; (3) set $\log_{10} N(d_{Max}) = -0.5 \log_{10}(10\text{ m}) + \log_{10} a = 0$ to determine $\log_{10} a$; and (4) calculate N (faults with $d \leq 5$ mm) ≈ 63. If $c \approx 0.6$, N (faults with $d \leq 5$ mm) ≈ 145. In either case, faults are more numerous in the real 500 m test line (even after subtracting possible strike-slip faults) than predicted by using the assumed value of the scaling parameter C_1''. Since small faults are unlikely to be over-sampled, the assumed value of C_1'' must be incorrect. Third, one can assume that this population resembles that in the strata above the coal seam, i.e. that the log N vs log d plot has a shallow slope for small-offset faults and a steep slope for large offset faults. Assuming a total number of faults ($N = 504$) and $c \approx 0.55$ (from Fig. 5), one sees that faults with 1–20 cm separations would need to have been under-sampled by a factor of 3, or their displacements would need to be underestimated by a factor of 3–10, in order to have the sample resemble that in Fig. 4. It is possible that faults with moderate offsets were either under-sampled severely, or that their true displacements are quite different from the measured separations. I believe that these possibilities are highly improbable. These three back-of-the-envelope calculations suggest that the slope on Fig. 4 is a reliable estimate of the one-dimensional size–frequency scaling parameter C_1''.

Thus, despite: (1) the uncertainty in equating the lineation direction and slip direction; (2) the uncertainty that arises because not all faults have lineations; and (3) the possible effects of a range of slip directions on faults, I infer here that, c, the slope of Fig. 4, is approximately equal to C_1'' of Marrett & Allmendinger (1991) or C_1 of Westaway (1994). The value of C_1'' for this fault population is markedly different from the typical value of this parameter, but it falls within a range of acceptable values (Marrett & Allmendinger 1991). In detail, of course, measured dip separations scale only in a general way with the true displacements on these faults. Inasmuch as fault separations do not scale uniformly with fault displacement, the log N vs log d plot in Fig. 4 cannot exactly mirror a displacement population for faults below the coal seam. Scaling parameters inferred from other 'displacement populations' that are compilations of heaves or throws on faults measured in seismic sections (e.g. Childs *et al.* 1990, Walsh *et al.* 1990, Marrett & Allmendinger 1992, Westaway 1994), where estimates of slip directions are rarely tightly constrained, may be similarly imprecise.

Changes in log N *vs log* d *plots correlated to fault size.* Marrett & Allmendinger (1991) argued that one-dimensional samples of fault populations yield systematic differences in counts of large faults, which extend across the brittle crust, and small faults, which do not extend across the brittle crust. Thus, while a fault population may explicitly follow power-law scaling, a log N vs log D plot derived from a one-dimensional sample, like the linear traverses used here, could have a non-linear form (see Marrett 1996). Wojtal (1994), using data compiled from two-dimensional profiles of faulted rocks, argued that within a limited sample area faults of different sizes follow different scaling laws, leading to stepped or faceted log N vs log D plots. The changes in fault behavior hypothesized by Wojtal (1994) occur at length scales of tens or hundreds of meters, where stratigraphic variations in rock behavior give rise to distinctions between 'large' and 'small' faults, not at a length scale of tens of kilometers, the length scale inferred to correlate with a change from unbounded to bounded growth of faults (Scholz & Cowie 1990) or with changes in slip characteristics of faults (e.g. Pacheco *et al.* 1992). Allmendinger (personal communication 1994) suggested that the size-related changes noted by Wojtal (1994) result from incomplete sampling and do not indicate a systematic change in scaling parameters with fault size. Nicol *et al.* (1996) argued, however, that systematic changes in the slopes of log N vs log D plots do correlate to fault size, suggesting that size-related changes in fault scaling laws are real. It is, then, important to examine the displacement populations considered here with the aim of separating real variations from artifacts due to sampling faults of different sizes.

Marrett & Allmendinger (1991) identified differences in the rates at which 'large' and 'small' faults are sampled that depend upon fault 'dimensionality': faults that cut the brittle crust are effectively two-dimensional features, whereas smaller faults are three-dimensional features. They showed (see also Westaway 1994) that for sample populations taken from a fault population

$$C_1' = C_1'' + 1/C_2 \tag{8}$$

and

$$C_1 = C_1'' + 2/C_2, \tag{9}$$

where C_1 is the scaling parameter relating the number (ΣN) of faults in a three-dimensional volume to fault displacement (D), C_1' is the slope of a log N vs log D plot derived from a sample collected at one lower dimension, i.e. two-dimensional sampling of three-dimensional faults, C_1'' is the slope of a log N vs D plot derived from a sample collected at two lower dimensions, i.e. one-dimensional sampling of three-dimensional faults, and C_2 is the scaling parameter relating fault displacement to fault length. Equations (8) and (9) provide a way to correct for size-related differences in the dimensionality of faults.

A one-dimensional sampling technique like that employed here will sample large and small faults at different rates. If, as suggested by Wojtal (1994), an individual stratum contains both 'large' faults, which cut entirely across that stratum, and 'small' faults, which are confined to that stratum, one can anticipate that the rates at which 'large' and 'small' faults are sampled within a restricted area mimic the rates at which large and small faults are sampled in regional studies. Drawing an analogy with the situation described by equation (8) suggests that the one-dimensional sampling rate for two-dimensional 'large' faults with a stratum, C_S', relates to the one-dimensional sampling rate for three-dimensional 'small' faults in that stratum, C_S'', by

$$C_S' = C_S'' + 1/C_2. \tag{10}$$

There is some disagreement on the precise value of C_2 (cf. Walsh & Watterson 1988, Cowie & Scholz 1990, Marrett & Allmendinger 1991), but $1 \leq C_2 \leq 2$.

The displacement population for faults above the coal seam (Fig. 5) has separate linear segments for faults with $d \leq 1.25$ m and faults with $d > 1.25$ m. The best-fit values for slopes for 'small' and 'large' faults on Fig. 5 are, respectively, $C_S'' = 0.53$ and $C_S' = 1.82$. Whether one assumes that $C_2 \approx 1.5$ (Marrett & Allmendinger 1991) and $1/C_2 \approx 0.67$ or one assumes that $C_2 = 1$ (Scholz & Cowie 1990, Clark & Cox 1996) and $1/C_2 = 1$, $C_S' \neq C_S'' + 1/C_2$. The difference in the rates of occurrence of 'small' and 'large' faults in this population is significant, indicating that faults with $d > 1.25$ m exhibit different size–frequency scaling than faults with $d \leq 1.25$ m. The break in slope at $d \approx 1.25$ m corresponds to faults whose lengths $\approx$ 100–150 m and whose heights $\approx$30–75 m (assuming length to height ratios of 2:1–3:1; Watterson 1986, Walsh & Watterson 1988). The inferred fault heights correspond to the thickness of the faulted strata above the coal seam (~30 m). It is possible that their growth was bounded (Scholz & Cowie 1990) by the coal horizon below and the shale horizon above, both of which probably were active as detachments while slip accrued on extension faults. If this were the case, faults with $d > 1.25$ m would be comparable to faults that extend across the brittle crust in regional studies. Alternatively, faults with $d > 1.25$ m may have exhibited slip characteristics different from the slip characteristics of smaller faults (cf. Pacheco *et al.* 1992, Wojtal 1994).

The effect of fault linkage on fault population evolution

If, in a limited area, geometrically and kinematically related faults of different sizes exhibit different scaling characteristics, one can no longer confidently extrapolate log N vs log d plots beyond the range of observation. Further analysis of the displacement population for extension faults above the coal seam provides, however, some insight to the implications of distinct linear trends on log N vs log d plots.

Using the values of c and $\log_{10} a$ determined from a least-squares regression of the data for faults with dip separations $\leq$ 1.25 m on Fig. 5, one can extrapolate $\log N = -c \log d - \log a$ to predict d_{Max} = 300–400 m, which is unreasonable in this structural setting. In the two-

dimensional road cut exposures, where rock faces are typically ~10 m tall, some faults intersected by the traverse line can be traced across the outcrop face to branch points with other faults (some of which also intersect the linear traverse). The overall frequency of faults with large separations, 24 faults with $d \geq 1$ m in 250 m along the outcrop trace, indicates a mean spacing of ~10 m. Individual large-offset faults typically make dihedral angles of 30–40° with the nearest neighboring large-offset fault. A straightforward trigonometric analysis that assumes planar faults, a mean spacing between adjacent large-offset faults of 10 m, and a dihedral angle between adjacent large-offset faults of 35° indicates that adjacent large-offset faults will intersect within 15–18 m of the traverse line. Unrecorded fault linkages undoubtedly occur in other parts of the section not exposed here.

Some linked faults have total displacement vs total length ratios that match the displacement vs length ratios of individual faults (Walsh & Watterson 1991, Dawers & Anders 1995), and could therefore follow the same displacement–length scaling laws as individual faults (Marrett & Allmendinger 1991). In order to take into account information on fault linkages visible in the two-dimensional exposure here. I recast the fault counts by considering any two or more faults that cross the traverse line and that join to be a single fault whose total displacement is the sum of the displacement of its component faults, and constructed a log N vs log d plot for the recast population (Fig. 7). This action reduced the total number of faults, thereby shifting the entire population downward along the log N axis, and created 'new' data points farther from the origin along the log d axis. The new points are unlikely to be precisely positioned because simply summing the observed offsets ignores any additional displacements due to rotation of beds in relay ramps. The log N vs log d plot in Fig. 7 still has a break in slope, but the knee occurs at $d \approx 1.9$ m. The slope of the curve for $d \leq 1.9$ m is slightly steeper ($c = 0.551$) while the slope of the curve for $d \geq 1.9$ m is slightly lower ($c' = 1.531$). Taking $C''_S = 0.55$, $C'_S = 1.53$, and $C_2 = 1$ (Scholz & Cowie 1990, Clark & Cox 1996), C'_S is nearly equal to $C''_S + 1/C_2$. By accounting for additional, unrecorded, links between faults, a log N vs log d plot for an 'adjusted' population composed of individual small faults and arrays of linked faults could adhere to uniform scaling parameters if the large, linked-fault arrays are essentially two-dimensional features and are sampled too frequently, i.e. if equation (10) holds and if C_2 has the appropriate value (Fig. 8). A complete accounting of fault linkages, which would require a complete three-dimensional picture of the faults in these strata, could yield a recast population with a less distinct break in slope or no break in slope at all (Fig. 8).

This examination underscores the meaning of faceted log N vs log d plots outlined by Wojtal (1994): provided that under-sampling can be discounted, a break in slope implies fault linkage and interaction. In the case considered here, where fault branch points are visible in the rock on either side of the traverse line, it is possible to adjust the displacement population to account for fault links and to argue that all members of the adjusted fault population exhibit the same scaling behavior. The hypothesis that a fault population remains fractal once faults link is not only intrinsically interesting, it provides tacit support for the inference that arrays or linked faults are geometrically and kinematically coherent (Walsh & Watterson 1991) and adhere to the same displacement–length scaling laws followed by individual faults (cf. Peacock & Sanderson 1991, Dawers & Anders 1995). On the other hand, the practical aspects of fault population analysis are difficult to assess in the context of adjustments for linked faults. Linear traverses, borehole data or drill core samples rarely indicate which faults link, and lacking that information there is no unique solution to which faults to combine to achieve proper adjustment of the displacement population. By hypothesizing links in faults, then, one has a means to adjust some or all of the log N vs log d data to comply with assumed scale invariance. Lacking the knowledge of specifically which faults to link, however, one cannot

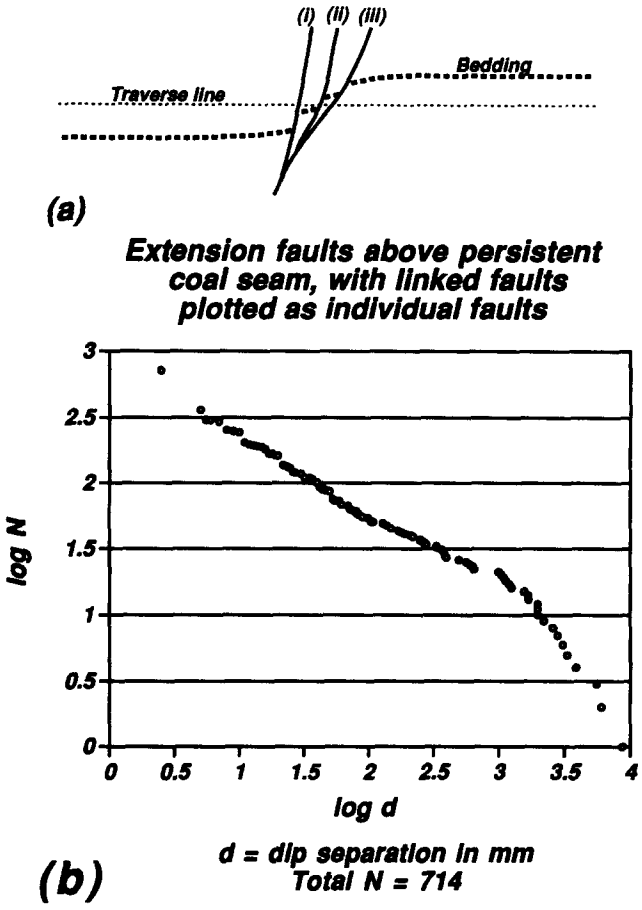

Fig. 7. (a) Cross-sectional sketch showing traverse line intersecting three faults (i, ii and iii) that link. This three fault array is equivalent to a single fault with an offset of bedding approximately equal to the sum of the offsets on the three individual faults. (b) Plot of log N vs log d for a population of 714 individual faults and arrays of linked faults in strata above persistent coal seam. This fault population was derived from the fault population shown in Fig. 5 by considering all faults that linked as fault arrays. The net separation of the fault array is the algebraic sum of the separations of the individual component faults. Data fall along two lines; least-squares regression gives −0.55 and −1.53 as the approximate slopes of the lines.

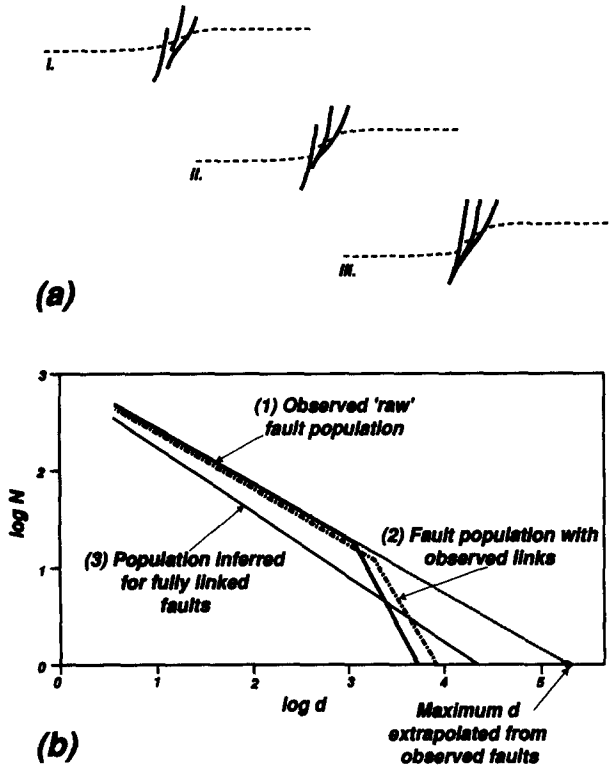

Fig. 8. (a) Three cross-sectional sketches showing the proposed evolution of a linked fault array, which has a net separation of bedding greater than any of its component faults. The formation of this linked array effectively replaces several faults in small offset classes by a single fault in a large offset class. (b) Comparisons of the log N vs log d plots for: (1) the faults above the coal seam intersected in a linear traverse across the outcrop (a sketch of the two best-fit lines from Fig. 5); (2) the fault population inferred for individual faults and linked fault arrays (a sketch of the two best-fit lines from Fig. 7); and (3) a sketch showing the possible appearance of the log N vs log d plot after adjusting for all fault linkages.

know what adjustments are appropriate, what are the intrinsic or true scaling parameters of the fault population, and one still lacks the confidence to extrapolate to larger or smaller length scales.

Fault linkage, population evolution and the relative importance of 'small' and 'large' faults

Fault populations that accommodate small strains typically have relatively steeply-sloped log N vs log d plots; fault populations that accommodate large strains typically have relatively shallowly-sloped log N vs log d plots (Kakimi 1980, Marrett & Allmendinger 1992, Wojtal 1994). This general observation holds for the low strain and high strain cases here (Figs. 4 and 5, respectively). Given the similarity in rock type, structural setting and fault geometry in these two cases, comparing these two populations could yield some insight to what causes such a change in fault population dynamics. Two factors become important in this comparison: (1) the development of 'large' faults that interact, whose growth is bounded, or whose slip characteristics differ from the slip characteristics of small fault; and (2) limits on the numbers of small faults within a rock volume. Both factors lead to increasing numbers of links between faults, which in turn leads to shallower slopes for the small-fault segments of log N vs log d plots and steeper slopes for the large-fault segments of plots.

Consider first the low strain fault population below the coal seam. The slope of the log N vs log d plot for this population, c = 0.812–0.857, is significantly different from the typical value of fault scaling parameters, $C_1'' \approx$ 0.5 (Marrett & Allmendinger 1991). The analysis above indicates, however, that c inferred from Fig. 4 is a reliable estimate of the estimate of C_1''. The excellent linear fit of the data on Fig. 4 supports the inference that a single scaling relationship holds for this population of high-angle faults.

The magnitude of the slope of the log N vs log d plot for faults above the coal seam (Fig. 5) is closer to the typical value for C_1'' ($\approx$ 0.5; Marrett & Allmendinger 1991). The analysis above, which accounts for links between faults, suggests however that C_1'' for this population may be higher than this measured value. Considering only the range of observed displacement values and the total number of faults sampled in this population, a value of $c \approx 0.8$ is required to produce a sufficiently large total number of faults in a 250 m test line (Fig. 9a). The large strain population above the coal seam consists of a significantly larger number of individual faults (745 faults encountered by a test line ~250 m long) than the small strain population below the coal seam (504 faults encountered by a test line ~500 m long). Large-offset faults with a spacing roughly equal to those intersected by the test line are also visible in inaccessible exposures of strata above the coal seam well to the east of A on Fig. 2. Thus, the large number of faults in the 'high-strain' population is not a product of fault clustering. New faults apparently nucleated as strain magnitude increased in the strata above the coal seam. Nucleation is required to maintain the slope of a log N vs log d plot as the largest faults in the population grow (fig. 8 in Wojtal 1994). Marrett & Allmendinger (1990, 1991) argue that as long as individual faults in an area exhibit a characteristic geometric shape (e.g. Walsh & Watterson 1988, Cowie & Scholz 1992a,b, Scholz *et al.* 1993), fault size distributions will follow power-law scaling. At low strain states where fault interactions are rare, as is the case below the coal seam, fault populations could exhibit the same size–frequency scaling behavior at different stages. The relatively large total number of faults suggests that, at a comparably low strain stage during its development, the fault population above the coal seam had a c value similar to that observed below the coal seam. The early stages of fault population development may have then been characterized by relatively steep slopes on log N vs log d plots (e.g. a and b on Fig. 9b).

In settings where fault size is limited (i.e. by the thickness of a particular bed or the thickness of the 'brittle' crust), the dynamics of the growth of individual faults are likely to change once faults extend across the deforming layer. Faults will then tend toward rectangular rather than elliptical shapes, and their displacement profiles will tend to develop flat tops. This change in the geometry of individual faults suggests that faults may not

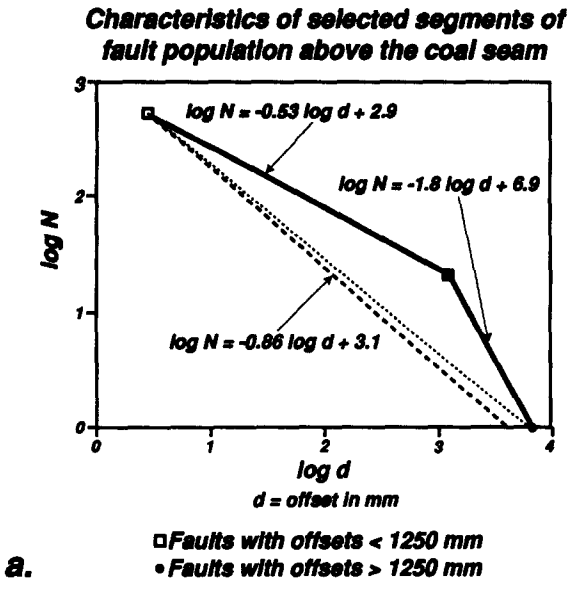

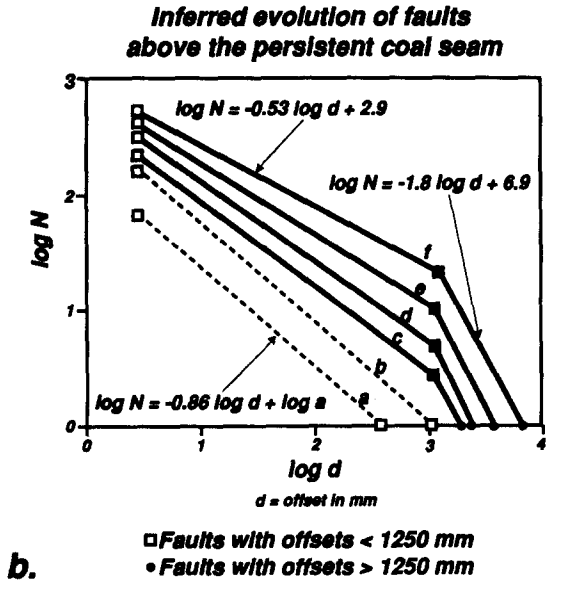

Fig. 9. (a) Comparison of log N vs log d plots of the small-strain and large-strain fault populations. The dashed line denotes small-strain displacement population below coal seam. Solid lines denote the 'small' fault and 'large' fault linear trends of the high-strain displacement population above the coal seam. The dotted line connecting the largest separation fault to the smallest separation class has a slope nearly equal to 0.86, suggesting that C_1'' may have initially been larger than 0.5 in order to generate the large number of faults observed in these strata. (b) A series of log N vs log d plots showing the proposed evolution of the fault population above the persistent coal seam as strains increased, *a* represents an early stage of development not seen in these exposures. *b* shows the population at a stage comparable to that observed in strata below the persistent coal seam. *c*, *d* and *e*, show the progressive effects of links between increasing numbers of faults. *f* is the fault population observed in the strata above the coal seam, i.e. Fig. 5.

be as efficient as accommodating elongation. Fault linkage or the development of geometrically coherent arrays of faults (Walsh & Watterson 1991) could, however, facilitate continued increase in strain magnitude.

Strata above the coal seam, for example, had bed-parallel slip zones immediately above and below, meaning that there were impediments to continued slip on individual faults once their tips neared either the bottom or top of the strata. Once a large-offset fault attained this size, it could contribute to deformation more effectively by linking or otherwise interacting with other faults. A log N vs log d plot adjusted for fault linkage could still conform to a single slope, but unadjusted data are likely to possess distinct 'small' and 'large' fault segments. In sample populations derived from linear traverses, fault linkage will be manifest as a break in the slope of a log N vs log d plot (e.g. stages *c* and *d* on Fig. 9b).

Continued growth of the largest-offset faults or linked fault systems requires further nucleation of small faults in order to maintain the slope of the log N vs log d plot. Wojtal & Mitra (1986) and Westaway (1994) have noted, however, the numbers of small faults that may form within a volume of rock under particular deformation conditions are limited. A limit on the number of small fault effectively pins the small-fault end of a log N vs log d plot, and sets the stage for a reduction in slope for the small-fault segment of the log N vs log d plot. Continued fault nucleation is also likely to lead to increased fault linkage. Some arrays of linked faults may have sufficiently low degrees of surface complexity that they are favored for additional slip increments. In such cases, fault linkage will both reduce the number of individuals in smaller separation classes and increase the number of individuals in larger separation classes, thereby moving data points from the upper left to the lower right on log N vs log d plots. The net result is a reduction of slope for the small-fault segments of log N vs log d plots (e.g. *e* and *f* on Fig. 9). These two factors may account for the different slopes for small-offset faults on Figs. 4 and 5.

In generalizing these observations to other fault populations, the absolute size of the faults described here may be significant. Only the largest individual faults or arrays of linked faults in the populations described here have sufficiently large offsets to be visible on seismic sections or to appear on most fault maps. Not all faults of this size need have the same likelihood for continued growth. If some individual faults develop relatively weak fault-rocks (Mitra 1984, Wojtal & Mitra 1986) or some arrays of linked faults are relatively smooth, i.e. have relatively low surface complexities (Okubo & Aki 1987), they might be favored for continued slip. If other 'large' individual faults lack weak fault rocks or if other 'large'-offset arrays of linked faults are more irregular, i.e. have relatively high surface complexities, they might be relatively unfavored for continued slip. Differences in the slip characteristics of faults or arrays of faults in this population may lead to the concentration of slip on a specific subset of the initial population, leading to different scaling behavior for those faults as total strain accrues. The difference in fault scaling behavior related to fault size hypothesized by Nicol *et al.* (1996) may be an indirect effect of a difference in fault scaling behavior related to total strain because large faults correlate with greater strain magnitudes. The faults observed in seismic sections or maps are likely to consist primarily of those relatively favored for continued slip by the occur-

rence of weak fault rocks or by lower overall surface complexity.

Fault linkage is then key to the changes in the character of log N vs log d plots. It is not clear whether or not fault populations exhibit different behavior in low strain and high strain settings or whether this apparent change can be accounted for by envisioning fault links. The development of numerous faults is, however, a mesoscopic to macroscopic structural change that alters the subsequent mechanical behavior of rocks (e.g. Wojtal & Mitra 1986). If the material properties of faulted rock differ from those of unfaulted rock, the two will exhibit different scaling characteristics (Watterson 1986, Walsh & Watterson 1988). In addition, if some large faults are zones of preferential localization of slip (Mitra 1984, Wojtal & Mitra 1986) or some large arrays of linked fault possess lower degrees of surface complexity than other arrays of linked fault strands (Okubo & Aki 1987, Wojtal 1994), they could exhibit different scaling behavior. In any case, it is likely that log N vs log d plots from large strain settings are not reliable in assessing the magnitude of the initial scaling parameters for fault populations. 'Adjusting' log N vs log d plots enables a single scaling law to apply to different stages in the development of a fault population, even after faults link together to form arrays. One motivation to adjust displacement populations by envisioning fault links is an *a priori* assumption that faults follow a single scaling law, and adjusting data to account for links removes any evidence that contradicts this assumption. The need for adjustment renders it impractical to determine the intrinsic or true scaling parameters from displacement populations, particularly from those collected using one-dimensional sampling techniques.

CONCLUSIONS

In strata near the top of a ~75 m thick deformed layer above the Cumberland Plateau thrust fault, two distinct populations of faults developed at high angles to bedding. Both fault populations accommodate subhorizontal elongation. Elongation of strata below a persistent coal seam is $\leq 1\%$. Elongation of strata above the coal seam is about 12%. This contribution considers size–frequency data collected along linear traverses across faults in each unit. A plot of log N (size rank) vs log d (dip separation measured in mm) for extension faults from the strata subjected to small strains supports an inference that all sizes of faults in this population exhibit the same scaling characteristics. The log N vs log d plot for extension faults from the strata subjected to large strains has a faceted appearance, with small- and large-separation faults defining distinct linear trends. The different linear trends are not an artifact of sampling in this example, but indicate that faults with different sizes exhibited different scaling behavior. The demonstration that faceted log N vs log d plots occur in some settings underscores the need for exercising caution in using these plots to estimate the frequencies of faults outside the range of observation or to estimate the relative magnitudes of strain accommodated by faults of different sizes.

Several of the large-offset faults in the high-strain fault population link with other small- or large-offset faults in the sample. If one assumes that linked faults constitute arrays that are geometrically-coherent to individual faults, one can derive an 'adjusted' fault population composed of individual faults and fault arrays. This adjusted fault population has fewer small-offset faults than the sampled population, and the magnitudes of total offset across fault arrays exceed the magnitude of the largest individual fault in the sampled population. The adjusted population composed of arrays of linked faults and isolated small faults here has a less-faceted appearance on a log N vs log d plot. This adjusted population may, in fact, conform with a single scaling relationship for all sizes of faults or fault arrays. This suggests that the faceted appearance of a log N vs log d plot is consistent with linkage between large offset faults. In most cases, however, it is unlikely that one will know which faults link to form arrays. Thus, it is unlikely that one can adjust a typical one-dimensional sample of a fault population to determine its true or intrinsic scaling parameters.

The analysis of fault linkage here shows that fault linkage leads to lower slopes on log N vs log d plots. Fault linkage is probably an important mechanism leading to the relatively low slopes of log N vs log d plots in large strain settings when compared with those in small strain settings. This analysis of the effects of fault linkage on log N vs log d plots indicates, further, that log N vs log d plots in large strain settings may not be as highly reliable for testing the hypothesis of power-law scaling and are not reliable for assessing the initial magnitudes of scaling parameters for fault populations.

Acknowledgements—I learned much at the Fault Populations Special Meeting of the Tectonic Studies Group, and thank Patience Cowie, Ian Main and Rob Knipe for their work in planning and running the meeting. I also thank Andrew Nicol, Chris Mansfield and Patience Cowie for careful reviews of this work and constructive critical comments. Finally, I thank Wendy Kozol for her continued important support.

REFERENCES

Arthaud, F. 1969. Méthode de détermination graphique des directions de raccourassement, d'allongement et intermédiare d'une population des failles. *Bull. Soc. géol. Fr.* **XI**, 729–737.

Cartwright, J. A., Trudgill, B. D. & Mansfield, C. S. 1995. Fault growth by segment linkage: an explanation for scatter in maximum displacement and trace length data from the Canyonlands grabens of SE Utah. *J. Struct. Geol.* **17**, 1319–1326.

Childs, C., Walsh, J. J. & Watterson, J. 1990. A method for estimation of the density of fault displacements below the limits of seismic resolution in reservoir formations. In: *North Sea Oil and Gas Reservoirs—II* (edited by Buller, A. T. *et al.*). Graham & Trotman, London, 309–318.

Cowie, P. A. & Scholz, C. H. 1992a. Physical explanation for displacement–length relationship of faults using a post-yield fracture mechanics model. *J. Struct. Geol.* **14**, 1133–1148.

Cowie, P. A. & Scholz, C. H. 1992b. Displacement–length scaling relationship for faults: data synthesis and discussion. *J. Struct. Geol.* **14**, 1149–1156.

Clark, R. M. & Cox, S. J. D. 1996. Displacement–length scaling relationships for faults: a modern regression approach. *J. Struct. Geol.* **18**, 147–152.

Dawers, N. & Anders, M. H. 1995. Displacement–length scaling and the fault linkage. *J. Struct. Geol.* **17**, 607–614.

Harris, L. D. & Milici, R. C. 1977. Characteristics of thin-skinned style of deformation in the southern Appalachians, and potential hydrocarbon traps. *Prof. Pap. U.S. geol. Surv.* **1018**, 1–40.

Hull, J. 1988. Thickness–displacement relationships for deformation zones. *J. Struct. Geol.* **10**, 431–435.

Jackson, P. & Sanderson, D. J. 1992. Scaling of fault displacements from the Jadajoz-Córdoba shear zone, SW Spain. *Tectonophysics* **210**, 179–190.

Kakimi, T. 1980. Magnitude–frequency relation for displacement of minor faults and its significance in crustal deformation. *Bull. geol. Surv. Jap.* **31**, 467–487.

Kamb, B. 1959. Petrofabric observations from Blue Glacier, Washington, in relation to theory and experiment. *J. geophys. Res.* **64**, 1889–1909.

Marrett, R. 1996. Aggregate properties of fracture populations. *J. Struct. Geol.* **18**, 169–178.

Marrett, R. & Allmendinger, R. W. 1990. Kinematic analysis of fault-slip data. *J. Struct. Geol.* **12**, 973–986.

Marrett, R. & Allmendinger, R. W. 1991. Estimates of strain due to brittle faulting: sampling of fault populations. *J. Struct. Geol.* **13**, 735–738.

Marrett, R. & Allmendinger, R. W. 1992. Amount of extension on "small" faults: An example from the Viking graben. *Geology* **20**, 47–50.

Milici, R. C. 1963. Low-angle overthrust faulting, as illustrated by the Cumberland Plateau–Sequatchie Valley fault system. *Am. J. Sci.* **261**, 815–825.

Mitra, G. 1984. Brittle to ductile transition due to large strains along the White Rock thrust, Wind River Mountains, Wyoming. *J. Struct. Geol.* **6**, 51–61.

Nemcok, M. & Lisle, R. J. 1995. A stress inversion procedure for polyphase fault/slip data sets. *J. Struct. Geol.* **17**, 1445–1453.

Nicol, A., Walsh, J. J., Watterson, J. & Gillespie, P. A. 1996. Fault size distributions — are they really power-law? *J. Struct. Geol.* **18**, 191–197.

Norris, D. K. 1958. Structural conditions in Canadian coal mines. *Bull. geol. Surv. Can.* **44**.

Okubo, P. G. & Aki, K. 1987. Fractal geometry in the San Andreas fault system. *J. geophys. Res.* **92**, 345–355.

Pacheco, J. F., Scholz, C. H. & Sykes, L. R. 1992. Changes in frequency–size relationship from small to large earthquakes. *Nature* **355**, 71–73.

Peacock, D. C. P. & Sanderson, D. J. 1991. Displacement, segment linkage, and relay ramps in normal fault zones. *J. Struct. Geol.* **15**, 721–733.

Pollard, D. D., Salzer, S. D. & Rubin, A. M. 1993. Stress inversion methods: are they based on faulty assumptions. *J. Struct. Geol.* **15**, 1045–1054.

Price, R. A. 1967. The tectonic significance of mesoscopic subfabrics in the south Rocky Mountains of Alberta and British Columbia. *Can. J. Earth Sci.* **4**, 39–70.

Ramsay, J. G. & Huber, M. I. 1983. *The Techniques of Modern Structural Geology. Volume* I: *Strain Analysis*. Academic Press, London.

Redmond, J. L. 1972. Null combination in fault interpretation. *Bull. Am. Ass. Petrol. Geol.* **56**, 150–166.

Rodgers, J. 1953. Geologic map of East Tennessee with explanatory text. *Tenn. Div. of Geol. Bull.* **58**, part II.

Scholz, C. H. & Cowie, P. A. 1990. Determination of total strain from faulting. *Nature* **346**, 837–839.

Scholz, C. H., Dawers, N. H., Yu, J.-Z., Anders, M. H. & Cowie, P. A. 1993. Fault growth and fault scaling laws: preliminary results. *J. geophys. Res.* **98**, 21,951–21,961.

Twiss, R. J. & Moores, E. M. 1992. *Structural Geology*. W. H. Freeman & Co., New York.

Underwood, E. E. 1970. *Quantitative Stereology*. Addison-Wesley, Reading, Massachusetts.

Villemin, T. & Sunwoo, C. 1987. Distribution logarithmique self-similaire des rejets et des longeurs de failles: Exemple du Bassin Houllier Lorrain. *C. r. Acad. Sci. Paris* **305**, 1309–1312.

Walsh, J. J. & Watterson, J. 1988. Analysis of the relationship between displacements and dimensions of faults. *J. Struct. Geol.* **10**, 239–247.

Walsh, J. J. & Watterson, J. 1991. Geometric and kinematic coherence and scale effects in normal fault systems. In: *The Geometry of Normal Faults* (edited by Roberts, A. M., Yielding, G. & Freeman, B.). *Spec. Publs geol. Soc. Lond.* **56**, 193–203.

Walsh, J. J., Watterson, J. & Yielding, G. 1991. The importance of small-scale faulting in regional extension. *Nature* **351**, 391–393.

Watterson, J. 1986. Fault dimensions, displacement, and growth. *Pure & Appl. Geophys.* **24**, 365–373.

Westaway, R. 1994. Quantitative analysis of populations of small faults. *J. Struct. Geol.* **16**, 1259–1274.

Wojtal, S. 1986. Deformation within foreland thrust sheets by populations of minor faults. *J. Struct. Geol.* **8**, 341–360.

Wojtal, S. 1989. Measuring displacement gradients and strains in faulted rocks. *J. Struct. Geol.* **11**, 669–678.

Wojtal, S. 1994. Fault scaling laws and the temporal evolution of fault systems. *J. Struct. Geol.* **16**, 603–612.

Wojtal, S. & Mitra, G. 1986. Strain hardening and strain softening in fault zones from foreland thrusts. *Bull. geol. Soc. Am.* **97**, 674–687.

Wojtal, S. & Mitra, G. 1988. Nature of deformation in fault rocks from Appalachian thrusts. In: *Geometries and Mechanisms of Thrusting, With Special Reference to the Appalachians* (edited by Mitra, G. & Wojtal, S.). *Spec. Pap. geol. soc. Am.* **222**, 17–33.

Wojtal, S. & Pershing, J. 1991. Paleostresses associated with faults of large offset. *J. Struct. Geol.* **13**, 49–62.